IEEE Access
Multidisciplinary ⋮ Rapid Review ⋮ Open Access Journal

Received September 30, 2021, accepted October 28, 2021, date of publication November 8, 2021,
date of current version November 16, 2021.

Digital Object Identifier 10.1109/ACCESS.2021.3126433

Hybrid Modelling and Control of a Class of Power Converters With Triangular-Carrier PWM Inputs

CAROLINA ALBEA[1], ANTONINO SFERLAZZA[2], (Member, IEEE), FABIO GÓMEZ-ESTERN[3], AND FRANCISCO GORDILLO[1]

[1]Department of System Engineering and Automatic Control, Universidad de Sevilla, 41092 Seville, Spain
[2]Department of Engineering, University of Palermo, 90128 Palermo, Italy
[3]Department of Engineering, Universidad de Loyola Andalucía, Seville, 41704 Dos Hermanas, Spain

Corresponding author: Carolina Albea (albea@us.es)

This work was supported in part by the Project PID2019-105890RJ-I00 and Project PID2019-109071RB-I00, in part by MCIN/ AEI /10.13039/501100011033/, in part by the ERDF A way of making Europe, in part by the Agence Nationale de la Recherche (ANR)–France under Grant ANR-18-CE40-0022-01, and in part by the ECSEL Joint Undertaking into the Project Frame of REACTION under Grant 783158.

ABSTRACT

In this paper, a new control design procedure for a class of power converters based on hybrid dynamical systems theory is presented. The continuous-time dynamics, as voltage and current signals, and discrete-time dynamics, as the on-off state of the switches, are captured with a hybrid model. This model avoids the use of averaged and approximated models and includes the PWM as well as the sample-and-hold mechanism, commonly used in the industry. Then, another simplified hybrid system, whose trajectories match with the original one, is selected to design the controller and to analyse stability properties. Finally, an estimation of the chattering in steady state of the voltage and current signals is provided. The results are validated through simulation and experiments.

INDEX TERMS Control of power converters, PWM, switched affine systems, hybrid dynamical systems, Lyapunov stability.

I. INTRODUCTION

Converter control has been widely studied by the electronics and control communities. Most of these studies deal with designing continuous-time control laws whose outputs are discretized by modulators. The most common modulator is the Pulse-Width Modulator (PWM) [1], [2]. Very often, this modulator is not considered in the converter control design and in the subsequent stability analysis. Instead, continuous-time approximate models, such as averaged models [3]–[5] are commonly used. These approaches have solved many practical problems and provided reasonably solid theoretical grounds, but these results might appear superficial when compared with the depth of analysis reached in other areas nowadays. Probably, the most relevant limitations are both the difficulty of quantifying the precision of the approximation resulting from the averaging procedure, and the fact that the properties of the control laws are only valid locally. In this way, it is known that PWM blocks have an effect on the output, [6], [7]. Mainly, the problem arises when the control designer ignores the discrete character of the signal, which is maintained constant for an elapsed time, possibly causing output jitter in steady state.

Recently, the control community has devoted efforts to the study of new hybrid control techniques [8], such as sliding mode control [9] or model predictive control [10] applied to power converters with the possibility of considering the continuous-time dynamics (voltage and current signals) and discrete-time dynamics (the functioning mode of the switches). This class of hybrid systems is modelled by switched affine state-space equations, where the constant matrices change depending on the state of the switches. Other hybrid controllers are presented in [11], [12], where the unique control action is the selection of an operating mode among a finite set of possibilities. In the latter reference, the problem is formulated in terms of the control of switched systems, whose modes are described by affine differential equations. However, it is possible to show that the obtained switching rule can be interpreted as a sliding mode control law where the sliding surfaces are implicitly determined in terms of the state space variables (current, voltage) and of the selected operating point [13]. On the other hand,

The associate editor coordinating the review of this manuscript and approving it for publication was Zheng H. Zhu.

relevant results on Hybrid Dynamical System (HDS) theory [14]–[18] have been applied to power converters. It also is worth to mention the design of hybrid controllers with minimum dwell-time guarantees [19]. Moreover, in [20]–[22] DC-DC as well as DC-AC power converters were controlled using this approach. The main feature in these references is the implementation of an aperiodic sampled-data based control signal with arbitrarily fast switching, and the possible induction of a Zeno behaviour. This issue is solved in [23], [24], where suitable formalisms relying on controlled switches with control inputs updated in a periodic or aperiodic manner are presented, without considering PWM. A hybrid control using HDS theory was proposed in [25] for a DC-AC converter. However, with most of these variants, which do not include PWM in the controller, the state of the switching devices can only be changed at the sampling instants. Notice that when a PWM is used, the manipulated control input can change in any instant inside the sampling period, with the only constraint in the maximum number of commutations inside this time interval. When the use of PWM is avoided, it is necessary to increase the sampling frequency to preserve a suited performance. Thus, the consideration of PWM in power converters using HDS theory is of interest. In [26], under some assumptions, it is proved for general systems that the solutions of an averaged system are suited approximations of the original one composed of a PWM. They mention power converters as systems that benefit from this result.

This paper proposes a new control law based on HDS models, avoiding the use of classical approximations derived from averaged systems and guaranteeing stability properties including non-linearities as PWM and sampling-and-hold mechanisms. A preliminary work regarding the direct design of controllers for power converters with PWM based on HDS is [27], where power converters with switched affine models are considered together with the PWM and sampling-and-hold mechanisms. Unlike this paper,

- the PWM carrier considered thereby was a sawtooth signal. Although this requires simpler analysis, it is not the most usual carrier signal in PWM for power converters, since it is well known that triangular carriers yield better results in many applications, in terms of harmonic distortion [28], [29].
- The study using HDS theory of triangular carriers for PWM is more involved than the one for sawtooth signals, due to the fact that the number of commutations in a PWM interval is increased (it is almost doubled). As it will be shown here, it is not only necessary to enlarge the jump set for the hybrid model, but the number of state variables must also be increased.
- A fictitious, simpler system is introduced in the present paper, and its behavior is proven to match the original system's at the sampling instants. This result is used to design a control law with stability guarantee for this system and to extend its validity to the original one.
- An estimation of the chattering in the steady-state signals is provided for the original hybrid model in the present work.

Experimental results verify the validity of the proposed control loop. Moreover, these validations are extended with an external loop to guarantee voltage output regulation, as it is commonly done in this kind of converters [30], [31].

This paper is organized as follows. The problem statement is given in Section II. Then, the hybrid general model of triangular-carrier PWM-based converters is presented in Section III. The main result is presented in Section IV, and Section V provides a discussion about parameter tuning effects. Section VI and Section VII present simulated and experimental results, respectively. Finally, the paper closes with a conclusion section.

Notation: Throughout the paper $\mathbb{N}$ denotes the set of natural numbers and $\mathbb{R}$ the set of real numbers, $\mathbb{R}^n$ the n-dimensional Euclidean space and $\mathbb{R}^{n\times m}$ the set of all real $n \times m$ matrices. The set of non-negative real numbers is denoted by $\mathbb{R}_{\geq 0}$. $M \succ 0$ (resp. $M \prec 0$) represents that M is a symmetric positive (resp. negative) definite matrix. 0 and I are the zero matrix and identity matrix respectively, of suited dimension. The operator $\|\cdot\|$ represents the Euclidean norm. $\mathrm{He}(M)$ is the Hermitian matrix of M, i.e. $\mathrm{He}(M) = (M+M^\top)$. Finally, $\mathrm{sat}_a^b(\phi)$ is the standard saturation function defined in $\mathbb{R} \mapsto [a, b]$.

II. PROBLEM STATEMENT

Many switched power converters can be modelled as switched affine systems, as follows

$$\dot{z} = A_\sigma z + \mathcal{B}_\sigma, \tag{1}$$

where $z \in \mathbb{R}^n$ contains the state variables, i.e. the continuous-time evolutions of the voltages and currents and $\sigma \in \{0, 1, 2, \ldots, N-1\}$ is the control input that represents the switching between the modes of the converter. Finally, A_σ and $\mathcal{B}_\sigma$ are matrices of suitable dimensions.

Model (1) covers many applications of power converters, such as the classical converters: buck, boost converter, quadratic boost converter, half bridge converter, boost inverter, etc. This set of power converters is modelled with two functioning modes, $N = 2$, and this is the case considered here, while it is possible to extend the results to converters with $N > 2$.

Generally, one can find in the literature that these systems are governed by continuous-time control laws [7], [32]–[34], i.e., $\sigma \in \{0, 1\}$ is modeled by continuous signals $\lambda \in [0, 1]$, obtained by using averaging approaches, and implemented in (1) by PWM, as depicted in Fig. 1, where $\kappa(x)$ represents a continuous control law whose output is limited to the interval [0, 1]. Furthermore, the control law is usually implemented in a digital device in discrete time by sampling the state of the converter $z(t)$ periodically. Thus, the value of λ in Fig. 1 is constant during each sampling interval. The PWM mechanism with a triangular carrier is illustrated in Fig. 2. For the sake of simplicity, in this paper, it is assumed that the

beginning of the triangular carrier period coincides with the time instants when the variables are measured, and the duty cycle is obtained from the controller equations.

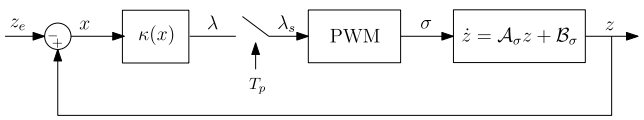

FIGURE 1. Feedback scheme.

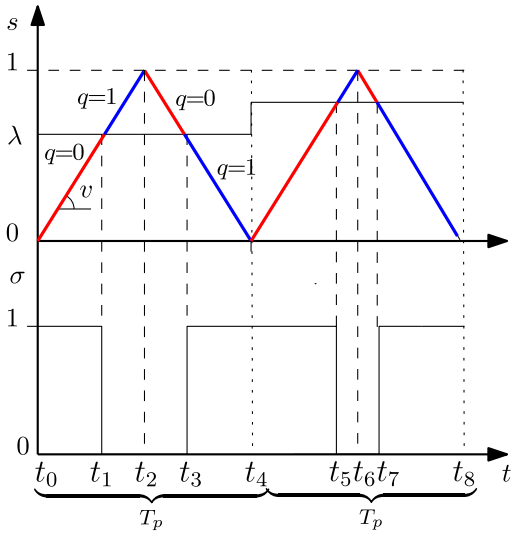

FIGURE 2. PWM mechanism. Top: T_p-periodic triangular carrier, s; λ is the duty cycle, v is the slope of the carrier s and q is a binary signal, taking value 0 when s is depicted in red, and 1 when in blue. Bottom: output of the PWM block, σ.

The control objective is to design a function $\lambda = \kappa(x) : \mathbb{R}^n \mapsto \mathbb{R}$ such that the control signal $\sigma(\lambda_s)$, modelled by a triangular carrier, ensures the convergence of z to a given operating point z_e. Due to the sampling mechanism, asymptotic convergence to z_e is not possible, and a chattering phenomenon is unavoidable. In any case, the desired operating point z_e must satisfy the following assumption.

Assumption 1: Given an operating point z_e there exists a $\lambda = \lambda_e \in [0, 1]$ such that the following equation holds,

$$0 = (A_0 + (A_1 - A_0)\lambda_e)z_e + \mathcal{B}_0 + (\mathcal{B}_1 - \mathcal{B}_0)\lambda_e. \quad (2)$$

This standard assumption for switched affine systems guarantees the existence of a switched signal for system (1), inducing an equilibrium in $z = z_e$ in the generalized sense of Filippov [35]. This means that, in steady state, σ is expected to be a periodic signal of period T_p, spending a time λT_p in mode 1 and $(1-\lambda)T_p$ in mode 0, corresponding to the convex combination of the right hand side of (2). Then, the time spent in each mode will be distributed in every sampling interval according to the used modulator. In this paper, it is assumed without loss of generality, that at $t = 0$ a triangular carrier as well as a sampling period start.

The error equation associated with (1) in each interval between sampling instants can be written as:

$$\dot{x} = A_\sigma x + B_\sigma, \quad (3)$$

where $x := z - z_e$ and $B_\sigma := \mathcal{B}_\sigma + A_\sigma z_e$ such that $B_{\lambda_e} = 0$, if Assumption 1 is satisfied.

Problem 1: Consider the switched system (1) with $N = 2$ and a PWM with a triangular carrier, as shown in Fig. 2. Then, the goals here are

- to model the closed-loop system considering its hybrid character, that is, the existence of both discrete-time and continuous-time signals, as well as the triangular-carrier PWM and sample-and-hold mechanism with a given periodic sampling time T_p.
- To design a new control law for the duty cycle λ.
- To achieve convergence of z to z_e and to analyse stability properties for both hybrid systems.
- To estimate the chattering of the voltages and currents in steady state.

III. HYBRID DYNAMICAL MODEL

In this section, the framework given in [14] about hybrid dynamical systems will be used to model the controlled system, considering continuous-time and discrete-time dynamics. Hence, the following hybrid dynamical model of the controlled switched system (3) is presented, considering a triangular carrier for the PWM mechanism,

$$\mathcal{H} : \begin{cases} \dot{\xi} & = f(\xi), \quad \xi \in \mathcal{C} \\ \xi^+ & \in g(\xi), \quad \xi \in \mathcal{D}, \end{cases} \quad (4)$$

being $\xi = [x\ s\ v\ \sigma\ q\ \lambda\ \tau]^\top \in \mathbb{H}$, such that, $\mathbb{H} := \mathbb{R}^n \times [0, 1] \times \{-2/T_p, 2/T_p\} \times \{0, 1\} \times \{0, 1\} \times [0, 1] \times [0, T_p]$. The maps f and g capture the continuous-time and discrete-time dynamics, respectively, and are defined as follows:

$$f(\xi) = \begin{bmatrix} A_\sigma x + B_\sigma \\ v \\ 0 \\ 0 \\ 0 \\ 0 \\ 1 \end{bmatrix},$$

$$g(\xi) = \begin{bmatrix} x \\ s \\ v - 2vq \\ (2\sigma - 1)q + (1 - \sigma) \\ 1 - q \\ (1 - q\sigma)\lambda + q\sigma\ \mathrm{sat}_0^1 \kappa(x) \\ (1 - q\sigma)\tau \end{bmatrix}. \quad (5)$$

with $\xi(0) = [x(0), 0, 2/T_p, \sigma(0), 0, \lambda(0), 0]$. The following sets

$$\begin{aligned} \mathcal{C}_1 &:= \{\xi \in \mathbb{H} : q = 1, \quad 0 \le s \le 1\} \\ \mathcal{D}_1 &:= \{\xi \in \mathbb{H} : q = 1, \quad s \le 0 \quad \text{or} \quad s \ge 1\} \\ \mathcal{C}_2 &:= \{\xi \in \mathbb{H} : q = 0, \quad sv \le \lambda v\} \\ \mathcal{D}_2 &:= \{\xi \in \mathbb{H} : q = 0, \quad sv \ge \lambda v\}, \end{aligned}$$

define the so-called flow and jump sets

$$\mathcal{C} := \mathcal{C}_1 \cup \mathcal{C}_2 \tag{6}$$
$$\mathcal{D} := \mathcal{D}_1 \cup \mathcal{D}_2. \tag{7}$$

This hybrid scheme (4)–(7) gathers the complete dynamics of the system. Indeed, the continuous-time dynamics of x evolves according to the switching of σ. The selection of the latter is given by a triangular modulator defined by s, v, q and λ. It is easy to see that s is a continuous-time triangular carrier (the signal shown in Fig. 2); v defines the slope of s; q is an artificial variable which takes values

$$q := \begin{cases} 0 \quad \text{if} \begin{cases} s < \lambda \text{ and } v \geq 0 \\ s \geq \lambda \text{ and } v \leq 0 \end{cases} \\ 1 \quad \text{if} \begin{cases} s > \lambda \text{ and } v \geq 0 \\ s \leq \lambda \text{ and } v \leq 0. \end{cases} \end{cases}$$

Variable $\lambda \in [0, 1]$ is the duty cycle, and $\kappa(x)$ is the control law, to be defined, that computes the value of signal λ in every sampling time. Inside the sampling intervals, λ is held constant. It is worth noting that the solutions to $\mathcal{H}$ are generalized Krasovskii solutions, not only in the map $f(\xi)$, but also in $g(\xi)$.

Solutions to $\mathcal{H}(f, G, \mathcal{C}, \mathcal{D})$ are given on the well-known hybrid time domain: $\text{dom}(\xi) \subset \mathbb{R}_{\geq 0} \times \mathbb{N}$, such that,

$$\text{dom}(\xi) = \bigcup_{j=0}^{\bar{j}-1} ([t_j, t_{j+1}], j), \tag{8}$$

for some sequence $0 = t_0 \leq t_1 \leq t_2 \leq \ldots \leq t_{\bar{j}}$ with $\bar{j}$ finite (being a compact set) or infinite.

In order to simplify the subsequent analysis, consider a second hybrid dynamical system, which is simpler than (4)–(7) and, as will be shown below, its trajectories match those of (4)–(7) at the sampling instants.

$$\mathcal{H}_p : \begin{cases} \dot{\xi}_p = f_p(\xi_p), & \xi_p \in \mathcal{C}_p \\ \xi_p^+ \in g_p(\xi_p), & \xi_p \in \mathcal{D}_p, \end{cases} \tag{9}$$

where $\xi_p = [x_p \ \lambda_p \ \tau_p]^\top \in \mathbb{H}_p$, such that, $\mathbb{H}_p := \mathbb{R}^n \times [0, 1] \times [0, T_p]$. The maps f_p and g_p capture both the continuous-time and discrete-time dynamics and are defined as follows:

$$f_p(\xi_p) = \begin{bmatrix} A_\lambda x_p + B_p \\ 0 \\ 1 \end{bmatrix},$$
$$g_p(\xi_p) = \begin{bmatrix} x_p \\ \text{sat}_0^1 \kappa(x_p) \\ 0 \end{bmatrix}, \tag{10}$$

where A_λ and B_p can be computed in different ways depending on the properties of the system. For this, consider a value of t corresponding to a sampling instant (when the period of the triangular carrier starts), that is, $q = 1$, $s = 0$ in system (4)–(7). It is clear that at this moment system (4)–(7) jumps. Consider a value of k such that t_k is equal to this time instant. By direct integration of the dynamics of x in $\mathcal{H}$ along the triangular carrier period (Fig. 2), starting from an initial condition $x(t_k)$ yields[1]

$$x(t_{k+1}) = e^{A_1 \frac{\lambda}{2} T_p} x(t_k) + (e^{A_1 \frac{\lambda}{2} T_p} - I) A_1^{-1} B_1 \tag{11}$$
$$x(t_{k+3}) = e^{A_0 (1-\lambda) T_p} x(t_{k+1}) + (e^{A_0 (1-\lambda) T_p} - I) A_0^{-1} B_0 \tag{12}$$
$$x(t_k + T_p) = e^{A_1 \frac{\lambda}{2} T_p} x(t_{k+2}) + (e^{A_1 \frac{\lambda}{2} T_p} - I) A_1^{-1} B_1, \tag{13}$$

being $t_{k+1} = t_k + T_p \frac{\lambda}{2}$ and $t_{k+3} = t_k + T_p (1 - \frac{\lambda}{2})$.

Then, the following assumption will explore different possibilities to compute A_λ (B_p will be considered later), from (11)–(13) such that the following holds

$$x(t + T_p) = e^{A_\lambda T_p} x(t) + (e^{A_\lambda T_p} - I) A_\lambda^{-1} B_p. \tag{14}$$

Assumption 2: Using the following definition

$$\Upsilon(\lambda) := e^{A_1 \frac{\lambda}{2} T_p} e^{A_0 \frac{(1-\lambda)}{2} T_p} e^{A_0 \frac{(1-\lambda)}{2} T_p} e^{A_1 \frac{\lambda}{2} T_p},$$

which arises from rewriting (11)–(13) as

$$x(t_k + T_p) = \Upsilon(\lambda) x(t_k) + (e^{A_\lambda T_p} - I) A_\lambda^{-1} B_p,$$

it will be assumed that one of the following conditions are verified by T_p and system matrices A_0 and A_1.

1 The sampling period T_p is sufficiently small such that $\|\Upsilon(\lambda) - I\| < 1$ for all $\lambda \in [0, 1]$.
2 The matrices A_0 and A_1 are commutative, i.e. $A_0 A_1 = A_1 A_0$. Under this condition, it is easy to prove that

$$\Upsilon(\lambda) = e^{(A_0 + (A_1 - A_0)\lambda) T_p}.$$

Now, for the definition of A_λ, there are two options.

- $A_\lambda := \log(\Upsilon(\lambda))/T_p$ if Assumption 2.1 holds, but Assumption 2.2 does not. The assumption guarantees the existence of the logarithmic matrix with real elements.
- $A_\lambda := A_0 + (A_1 - A_0)\lambda$ if Assumption 2.2 holds.

Remark 1: Note that in Assumption 2, the conditions would lead to exact results. However a less restrictive condition can provide an approximation of A_λ. Indeed, a first-order approximation of the Taylor series expansion of $\Upsilon(\lambda)$ with respect to T_p around $T_p = 0$ yields

$$\tilde{\Upsilon}(\lambda) \approx e^{(A_0 + (A_1 - A_0)\lambda) T_p} = e^{A_\lambda T_p}.$$

For the cases where these conditions are not satisfied, the search for an alternative to the matrix logarithm can be done using the Baker–Campbell–Hausdorff formula, but this will not be further investigated here.

For the definition of B_p in (10), using Eqs. (11)–(13) gives,

$$B_p := \left((e^{A_\lambda T_p} - I) A_\lambda^{-1} \right)^{-1} B_{d\lambda} = (e^{A_\lambda T_p} - I)^{-1} A_\lambda B_{d\lambda}$$
$$= A_\lambda (e^{A_\lambda T_p} - I)^{-1} B_{d\lambda}$$
$$B_{d\lambda} := e^{A_1 \frac{\lambda}{2} T_p} e^{A_0 (1-\lambda) T_p} (e^{A_1 \frac{\lambda}{2} T_p} - I) A_1^{-1} B_1$$

[1]This formulation is valid for $\lambda \in (0, 1)$ but can be extended to the cases $\lambda = 0$ and $\lambda = 1$ yielding the same results.

$$+e^{A_1\frac{\lambda}{2}T_p}(e^{A_0(1-\lambda)T_p}-I)A_0^{-1}B_0$$
$$+(e^{A_1\frac{\lambda}{2}T_p}-I)A_1^{-1}B_1.$$

For future uses, it is worth noting that, when $T_p \to 0$ (neglecting the second and higher order terms on T_p), this expression approaches to

$$B_{d\lambda} \to (B_0+\lambda(B_1-B_0))T_p = B_\lambda T_p, \tag{15}$$

where B_λ has been defined accordingly.

The flow and jump sets, are now

$$\mathcal{C}_p := \{\xi_p \in \mathbb{H}_p : \tau_p \in [0, T_p]\} \tag{16}$$
$$\mathcal{D}_p := \{\xi_p \in \mathbb{H}_p : \tau_p = T_p\}. \tag{17}$$

Note that system (9)–(10),(16)–(17), corresponds to a sampled system controlled with a sample-and-hold mechanism, and its relationship with system (4)–(7) is stated in the following proposition, which expresses that at the time instants when system $\mathcal{H}_p$ jumps, system $\mathcal{H}$ also jumps and at these instants $x = x_p$. For this, consider the pair (t, j_p) such that system $\mathcal{H}_p$ jumps (subscript p in j has been introduced in order to avoid confusion with the jumps of $\mathcal{H}$).

Proposition 1: Consider systems (4)–(7) and (9)–(10), (16)–(17), with the same initial condition, i.e., $x(0,0) = x_p(0,0)$ and with the same control law $\kappa(x) = \kappa(x_p), \forall x = x_p$. Moreover, consider that each subsystem is Hurwitz. Then, at the time instants when system (9)–(10) jumps, i.e., when $\xi_p(t, j_p) \in \mathcal{D}_p$, for a given j_p, system (4)–(7) also jumps, i.e., there exists an integer j such that $\xi(t, j) \in \mathcal{D}$. Furthermore, $x(t, j) = x_p(t, j_p)$.

Proof: We proceed by induction showing that if at a given time t when system (9)–(10) jumps, $x(t, j) = x_p(t, j_p)$ for certain values of j and j_p, then at the following jump of this system, the state verifies that $x(t_j+T_p, j+4) = x_p(t_j+T_p, j_p)$ (see Fig. 2).

For this, integrating the dynamics of x_p in (9)–(10) between two consecutive jumps and using Assumption 2 the following equation is reached

$$x_p(t+T_p) = e^{A_\lambda T_p}x_p(t) + (e^{A_\lambda T_p}-I)A_\lambda^{-1}B_p. \tag{18}$$

From (14), and because at $t = 0$ it holds that $x(0,0) = x_p(0,0)$. The proposition statement is proved by induction. □

In the next section, a control law will be designed for system (9)–(10), (16)–(17) with stability guarantee. By Proposition 1, application of this control law to system(4)–(7) will inherit the stability property at sampling instants. The behaviour inside the time interval between sampling times will be analysed afterwards.

In the sequel, possibly with abuse of notation, the symbols λ and τ, instead of, λ_p and τ_p will be used.

Notice that the flow equation that governs the dynamics of x_p in (9)–(10), (16)–(17), is

$$\dot{x}_p = A_\lambda x_p + B_p. \tag{19}$$

This equation plays a similar role to the one of averaged models used usually in power electronics. Indeed, the use of variable λ instead of σ avoids the use of a discrete control signal. Nevertheless, the proposed approach presents important differences:

- At sampling instants, the solution to (9)–(10), (16)–(17) matches exactly the solution to (4)–(7), as it has been stated in Proposition 1. In fact, the usual averaged model would be similar to (19) but with $A_\lambda = A_0 + \lambda(A_1 - A_0)$, instead of the logarithm definition above, and $B_p = B_0 + \lambda(B_1 - B_0)$, where the equality signs can be just an approximation depending on which case of Assumption 2 is satisfied. In the approximated case, some issues can appear, as has been reported in designs based in averaged modes [36], [37].
- Model (9)–(10),(16)–(17), takes care of the discrete-nature of the control action since the sample-and-hold mechanism is included in the model.

Notice also that the non-hybrid model (18) (or its continuous version $\dot{x}_p = A_\lambda x_p + B_p$) is not a "standard" affine problem since the transmission matrix $e^{A_\lambda T_p}$ (or A_λ) depends on the control input λ.

Now, rewriting the continuous and discrete-time dynamics of x_p will lead to a new Lyapunov function candidate. To do so, define $\Gamma_q = \left[\begin{smallmatrix} A_q & B_q \\ 0 & 0 \end{smallmatrix}\right]$, such that during the flows:

$$\frac{d}{dt}\begin{bmatrix} x_p \\ 1 \end{bmatrix} = \Gamma_q \begin{bmatrix} x_p \\ 1 \end{bmatrix}. \tag{20}$$

Hence, the following Lyapunov function candidate is considered

$$V(x_p, \lambda, \sigma, \tau) = \max\left\{W(x_p, \lambda, \sigma, \tau) - 1, 0\right\}, \tag{21}$$

where W is a quadratic function of $[x_p \;\; 1]^\top$, defined as follows,

$$W(x_p, \lambda, \sigma, \tau) := \begin{bmatrix} x_p & 1 \end{bmatrix} \mathcal{P}_\sigma(\lambda, \tau) \begin{bmatrix} x_p \\ 1 \end{bmatrix} \tag{22}$$

with

$$\mathcal{P}_0(\lambda, \tau) := e^{-\Gamma_0^\top \tau}\bar{P}e^{-\Gamma_0 \tau}$$
$$\mathcal{P}_1(\lambda, \tau) := e^{-\Gamma_1^\top(\lambda T_p - \tau)}e^{-\Gamma_0^\top \tau}\bar{P}e^{-\Gamma_0 \tau}e^{-\Gamma_1(\lambda T_p - \tau)}$$

and $\bar{P} := \left[\begin{smallmatrix} P & 0 \\ 0 & 0 \end{smallmatrix}\right]$, being $P \succ 0$ a symmetric matrix.

We will see below that this Lyapunov function candidate enjoys nice properties.

We are in position to define the compact attractor for which it is desired to establish uniform globally asymptotic stability (UGAS). This attractor set is

$$\mathcal{A} := \{\xi_p \in \mathbb{H}_p : \; V(x_p, \lambda, \tau) = 0\}. \tag{23}$$

Note that if the solution evolves in the interior of $\mathcal{A}$ in steady state, its associated x_p is bounded.

The particular hybrid arcs starting from the origin after a jump are defined as follows:

$$\mathcal{E}_\kappa = \left\{\xi_p \in \mathbb{H}_p : x_p(\tau,\lambda) = \begin{bmatrix} I & 0\end{bmatrix} e^{\Gamma_\lambda(\lambda T_p - \tau)} \begin{bmatrix} 0 \\ 1\end{bmatrix}, \lambda = \text{sat}_0^1\, \kappa(0)\right\}. \tag{24}$$

Note that these arcs start from $x_p = 0$ and describe a solution of x in the time arcs, $[t_{j_p}, t_{j_p+1}]$ with $(t_{j_p}, j_p) \in \text{dom}(\xi)$.

IV. MAIN RESULT

Inspired by [24], a controller is proposed for system (9)–(10), (16)–(17) providing stability guarantees of the compact attractor $\mathcal{A}$.

Theorem 1: Consider a λ_e associated with the operating point x_e such that Assumption 1 is satisfied and matrices $P \succ 0 \in \mathbb{R}^n$, $Q \succ 0 \in \mathbb{R}^n$ such that $Q \succ P$ and $M \succ P - Q \in \mathbb{R}^n$ satisfying

$$A_0^\top P + PA_0 \prec -Q, \tag{25}$$
$$A_1^\top P + PA_1 \prec -Q. \tag{26}$$

Consider system (9)–(10), (16)–(17), with control law

$$\kappa(x_p) \in \begin{cases} \lambda_e \left(1 + \frac{x_p^\top M x_p}{2B_0^\top P x_p}\right) & \text{if } B_0^\top P x_p \neq 0 \\ [0,\, 1] & \text{if } B_0^\top P x_p = 0, \end{cases} \tag{27}$$

Then, there exists a value $T_p^* > 0$ such that for $0 < T_p < T_p^*$ the following statements hold:

(i) $\mathcal{A}$ is UGAS.

(ii) $\mathcal{E}_\kappa$ is a subset of $\mathcal{A}$.

Proof: Hybrid system $\mathcal{H}_p(f_p, g_p, \mathcal{C}_p, \mathcal{D}_p)$ with control law (27) is well-posed, because it verifies:

- $\mathcal{C}_p$ and $\mathcal{D}_p$ are closed sets in $\mathbb{H}_p$.
- f_p is a continuous function, thus it is locally bounded and outer semi-continuous. Moreover, it is convex for each $\xi_p \in \mathcal{C}_p$.
- g_p is outer semi-continuous and locally bounded.

We will consider the proof item by item.

Proof of (i): The proof of this item proceeds by applying [38, Theorem 1]. Note that the Lyapunov function candidate, $V(x_p, \lambda, \tau)$ (21) is continuous in $\mathcal{C}_p \cup \mathcal{D}_p$ and locally Lipschitz near each point in $\mathcal{C}_p \backslash \mathcal{A}$. Moreover, $V(x_p, \lambda, \tau)$ is strictly positive definite with respect to $(\mathcal{C}_p \cup \mathcal{D}_p)\backslash\mathcal{A}$ and radially unbounded. Likewise, it verifies, by definition, $V(x_p, \lambda, \tau) = 0$, for all (x_p, λ, τ) in $\mathcal{A}$.

The next step of the proof is to ensure that the time derivative of V along flows outside of $\mathcal{A}$ is non positive (or more precisely in this case, equal to zero). More formally, the objective is to show that

$$\langle \nabla V(x_p, \lambda, \tau), f(x_p, \lambda)\rangle \leq 0, \quad \forall (x_p, \lambda, \tau) \in \mathcal{C}_p \backslash \mathcal{A}. \tag{28}$$

For any $(x_p, \lambda, \tau) \in \mathcal{C}_p \backslash \mathcal{A}$, it is clear, from its definition, that $V(x, \lambda, \tau) = W(x_p, \lambda, \tau) - 1$ getting

$$\begin{aligned} &\langle \nabla V(x_p, \lambda, \tau), f(x_p, \lambda)\rangle \\ &= \begin{bmatrix} x_p \\ 1\end{bmatrix}^\top \left(\dot\tau \frac{\partial}{\partial \tau}\mathcal{P}(\lambda,\tau) + \dot\lambda \frac{\partial}{\partial \lambda}\mathcal{P}(\lambda,\tau)\right) \\ &\quad \times \begin{bmatrix} x_p \\ 1\end{bmatrix} + 2\begin{bmatrix} x_p \\ 1\end{bmatrix}^\top \mathcal{P}(\lambda,\tau)\begin{bmatrix} \dot x_p \\ 0\end{bmatrix} \\ &= \begin{bmatrix} x_p \\ 1\end{bmatrix}^\top \left(\frac{\partial}{\partial \tau}\mathcal{P}(\lambda,\tau) + \mathcal{P}(\lambda,\tau)\text{He}\,(\Gamma_\lambda)\right)\begin{bmatrix} x_p \\ 1\end{bmatrix} = 0. \end{aligned}$$

The last equality comes from

$$\frac{\partial}{\partial \tau}\mathcal{P}(\lambda,\tau) + \mathcal{P}(\lambda,\tau)\,\text{He}(\Gamma_\lambda) = 0.$$

Next, let us analyse the second stability condition from [38, Theorem 1]. To do so, taking into account that the special structure of hybrid system (9)–(10) implies that the jumps occur periodically at the ordinary time instants $t = j_p T_p$ for $j_p \in \mathbb{N}$, the following notation will be adopted here according the hybrid time domain (8): $x_{p,j_p} = x_p(j_p T_p, j_p)$, $\lambda_{j_p} = \lambda(j_p T_p, j_p)$, $\tau_{j_p} = \tau(j_p T_p, j_p)$ that corresponds to the variables right before the jump at $t = j_p T_p$ and $\lambda_{j_p}^+ = \lambda(j_p T_p, j_p + 1)$, $\tau_{j_p}^+ = \tau(j_p T_p, j_p + 1)$ right after the same jump. In the same way, the definition $\Delta V = V(x_{p,j_p}^+, \lambda_{j_p}^+, \tau_{j_p}^+) - V(x_{p,j_p}, \lambda_{j_p}, \tau_{j_p})$ will be used. However, note that $x_{p,j_p}^+ = x_{p,j_p}$, $\tau_{j_p}^+ = 0$ and $\tau_{j_p} = T_p$.

Now, $\forall (x_p, \lambda, \tau) \in \mathcal{D}_p \setminus \mathcal{A}$ the following equations hold,

$$\begin{aligned} \Delta V &= W(x_{p,j_p}, \lambda_{j_p}^+, 0) - W(x_{p,j}, \lambda_{j_p}, T_p) \\ &= \begin{bmatrix} x_{p,j_p} \\ 1\end{bmatrix}^\top \left(\bar P - \Psi_{\lambda_{j_p}}^\top \bar P \Psi_{\lambda_{j_p}}\right)\begin{bmatrix} x_{p,j_p} \\ 1\end{bmatrix} \\ &= \begin{bmatrix} x_{p,j_p+1} \\ 1\end{bmatrix}^\top \left(\bar P - \Psi_{\lambda_{j_p+1}}^\top \bar P \Psi_{\lambda_{j_p+1}}\right)\begin{bmatrix} x_{p,j_p+1} \\ 1\end{bmatrix} \end{aligned}$$

being $\Psi_{\lambda_{j_p}} = e^{-\Gamma_0 T_p} e^{-\Gamma_1(\lambda T_p - T_p)}$.

Notice that the manipulable signal, $\lambda_{j_p+1} = \lambda_{j_p}^+$ has to be computed at $t = j_p T_p$. For this, it is convenient to write ΔV in terms of x_{p,j_p} instead of x_{p,j_p+1}. Hence, from (20), the following relationship is obtained

$$\begin{bmatrix} x_{p,j_p+1} \\ 1\end{bmatrix} = \Psi_{\lambda_{j_p}^+}\begin{bmatrix} x_{p,j_p} \\ 1\end{bmatrix}. \tag{29}$$

We have

$$\Delta V = \begin{bmatrix} x_{p,j_p} \\ 1\end{bmatrix}^\top \left(\bar\Psi_{\lambda_{j_p}}^\top \bar P \bar\Psi_{\lambda_{j_p}} - \bar P\right)\begin{bmatrix} x_{p,j_p} \\ 1\end{bmatrix}. \tag{30}$$

being $\bar\Psi_{\lambda_{j_p}} := \Psi_{\lambda_{j_p}}^{-1}$. We highlight that $\lambda_{j_p}^+$, which depends on x_{p,j_p} according to the definition of $\mathcal{H}_p$, is associated with the value of x_p at the jump instant. Indeed, $(x_{p,j_p}, \lambda_{j_p}^+, 0)$ refers here to the initial value in each hybrid arc. In the sequel, possibly with abuse of notation, λ and x_p will be used to represent $\lambda_{j_p}^+$ and x_{p,j_p}, respectively.

From (30), it is not easy to verify that $\Delta V < 0$. However, only small values of T_p are of interest, and hence, one just can analyse the following limit

$$\lim_{T_p \to 0} \Delta V = \lim_{T_p \to 0} \begin{bmatrix} x_p \\ 1\end{bmatrix}^\top \left(\bar\Psi_{\lambda_{j_p}}^\top \bar P \bar\Psi_{\lambda_{j_p}} - \bar P\right)\begin{bmatrix} x_p \\ 1\end{bmatrix}.$$

When $T_p \to 0$, the following approximation can be used

$$\bar{\Psi}_{\lambda_{jp}} \approx \begin{bmatrix} I + A_{\lambda^+} T_p & B_{\lambda^+} T_p \\ 0 & 1 \end{bmatrix}, \tag{31}$$

with $B_{\lambda^+} := B_0 + (B_1 - B_0)\lambda^+$. Then, it holds that

$$\begin{aligned}
&\lim_{T_p \to 0} \Delta V \\
&= \lim_{T_p \to 0} \begin{bmatrix} x_p \\ 1 \end{bmatrix}^\top \left(\bar{P} - \left(e^{-\Gamma_{\lambda^+} T_p} \right)^\top \bar{P} e^{-\Gamma_{\lambda^+} T_p} \right) \begin{bmatrix} x_p \\ 1 \end{bmatrix} \\
&= \lim_{T_p \to 0} \begin{bmatrix} x_p \\ 1 \end{bmatrix}^\top \left(\bar{P} - \begin{bmatrix} P - \mathrm{He}(PA_{\lambda^+}) T_p & -PB_{\lambda^+} T_p \\ -B_{\lambda^+}^\top P T_p & 1 \end{bmatrix} \right) \begin{bmatrix} x_p \\ 1 \end{bmatrix} \\
&= \lim_{T_p \to 0} x_p^\top \mathrm{He}(PA_{\lambda^+}) x_p T_p + 2 x_p B_{\lambda^+}^\top P x_p T_p = 0,
\end{aligned} \tag{32}$$

which is achieved neglecting T_p^2 terms, both in (31) and in (32).

On the other hand, in order to evaluate the behavior of $\lim_{T_p \to 0} \Delta V$ for small T_p the following computation holds,

$$\begin{aligned}
&\lim_{T_p \to 0} \frac{\Delta V}{T_p} \\
&= x_p^\top \mathrm{He}(PA_{\lambda^+}) x_p + 2 B_{\lambda^+}^\top P x_p \\
&= x_p^\top \mathrm{He}(PA_{\lambda^+}) x_p + 2 B_0^\top P x_p + 2\lambda^+ (B_1 - B_0)^\top P x_p \\
&= x_p^\top \mathrm{He}(PA_{\lambda^+}) x_p + 2 \left(1 - \frac{\lambda^+}{\lambda_e} \right) B_0^\top P x_p.
\end{aligned} \tag{33}$$

The last step is reached from the next property

$$B_0 + (B_1 - B_0)\lambda_e = 0 \Rightarrow B_1 = -\frac{1 - \lambda_e}{\lambda_e} B_0, \tag{34}$$

stemmed from Assumption 1 and the error equation (3).

It is worth to remind that $\lambda^+ \in [0, 1]$. Now, consider that $B_0^\top P x_p = 0$, then

$$\lim_{T_p \to 0} \frac{\Delta V}{T_p} = x_p^\top \mathrm{He}(PA_{\lambda^+}) x_p < -x_p^\top Q x_p \tag{35}$$

The last condition stems from the fact that LMIs (25)–(26) are satisfied. Now, taking into account $B_0^\top P x_p \neq 0$, there are three distinct cases:

- $0 < \lambda^+ < 1$: Inserting (27) in (33), applying conditions LMI (25)–(26), $M \succ P - Q$ given in the Theorem statement and assuming that λ^+ is not saturated in (33), yields

$$\begin{aligned}
&\lim_{T_p \to 0} \frac{\Delta V}{T_p} \\
&= x_p^\top \mathrm{He}(PA_{\lambda^+}) x_p - x_p^\top M x_p \\
&< -x_p^\top (Q + M) x_p < -x_p^\top P x_p < 0 \quad \forall \xi_p \in \mathcal{D}_p \backslash \mathcal{A}.
\end{aligned}$$

- $\lambda^+ = 0$: This case takes place when $\kappa(x_p) \leq 0$, being (33) equal to

$$\lim_{T_p \to 0} \frac{\Delta V}{T_p} = x_p^\top \mathrm{He}(PA_0) x_p + 2 B_0^\top P x_p. \tag{36}$$

Note that there are two possibilities, either $M \succeq 0$ or $Q \preceq M \preceq 0$. First, let us consider $M \succeq 0$. Here, the saturation in $\lambda^+ = 0$ is reached if $2B_0^\top P x_p < 0$ (necessary for the argument of (27) to be negative or zero), being (36) negative $\forall \xi_p \in \mathcal{D}_p \backslash \mathcal{A}$ from the fact that condition (25) is satisfied. Finally, from applying $P \succ Q$, (36) yields

$$\lim_{T_p \to 0} \frac{\Delta V}{T_p} < -x_p^\top Q x_p < -x_p^\top P x_p.$$

Secondly, if $Q \preceq M \preceq 0$, then

$$\lambda_e \left(1 + \frac{x_p^\top M x_p}{2 B_0^\top P x_p} \right) \leq 0 \Rightarrow -x_p^\top M x_p \geq 2 B_0^\top P x_p$$

which implies

$$\begin{aligned}
\lim_{T_p \to 0} \frac{\Delta V}{T_p} &= x_p^\top \mathrm{He}(PA_0) x_p + 2 B_0^\top P x_p \\
&\leq x_p^\top \mathrm{He}(PA_0) x_p - x_p^\top M x_p \\
&< -x_p^\top (Q + M) x_p
\end{aligned}$$

Consequently, from $M \succ P - Q$ the following holds

$$\lim_{T_p \to 0} \frac{\Delta V}{T_p} < -x_p^\top P x_p < 0 \quad \forall \xi_p \in \mathcal{D}_p \backslash \mathcal{A}.$$

- $\lambda^+ = 1$: In this case, corresponding to the case when $\kappa(x_p)$ is saturated in its upper bound, (33) yields

$$\lim_{T_p \to 0} \frac{\Delta V}{T_p} = x_p^\top \mathrm{He}(PA_1) x_p + 2 B_1^\top P x_p. \tag{37}$$

Once again, two situations are particularized, $M \succeq 0$ as well as $Q \preceq M \preceq 0$. The saturation of the expression of $\kappa(x_p)$ at $\lambda^+ = 1$ with $M \succeq 0$ can only happen because $2B_0^\top P x_p > 0$, which implies from the equilibrium equation (34)

$$2 B_1^\top P x_p = -2 \frac{1 - \lambda_e}{\lambda_e} B_0^\top P x_p < 0. \tag{38}$$

Therefore, (37) becomes

$$\lim_{T_p \to 0} \frac{\Delta V}{T_p} < -x_p^\top Q x_p < -x_p^\top P x_p.$$

Now, for the case $Q \preceq M \preceq 0$ and noting that

$$\lambda_e \left(1 + \frac{x_p^\top M x_p}{2 B_0^\top P x_p} \right) \geq 1,$$

which yields the following condition

$$x_p^\top M x_p \leq 2 \frac{1 - \lambda_e}{\lambda_e} B_0^\top P x_p = -2 B_1^\top P x_p.$$

Then,

$$\begin{aligned}
\lim_{T_p \to 0} \frac{\Delta V}{T_p} &= x_p^\top \mathrm{He}(PA_0) x_p + 2 B_1^\top P x_p \\
&- < x_p^\top (Q + M) x_p < -x_p^\top P x_p.
\end{aligned}$$

Hence, for a given $M \succeq 0$ or $Q \preceq M \preceq 0$, it holds that

$$\lim_{T_p \to 0} \frac{\Delta V}{T_p} < -x_p^\top P x_p < 0 \quad \forall \xi_p \in \mathcal{D}_p \backslash \mathcal{A}$$

The last step is to prove that $\mathcal{A}$ is an invariant set, i.e., $g(\mathcal{A} \cap \mathcal{D}_p) \subset \mathcal{A}$ (remember that W does not change when $(x_p, \lambda, \tau) \in \mathcal{C}_p \cup \mathcal{D}_p$). To do so, remember that the following expression has been obtained

$$W(x_p, \lambda^+, 0) - W(x_p, \lambda, T_p) < -x_p^\top P x_p.$$

Moreover, note that $W(x_p, \lambda^+, 0) = x_p^\top P x_p$. Then, some manipulations yield

$$W(x_p, \lambda^+, 0) < \frac{1}{2} W(x_p, \lambda, T_p).$$

Therefore, $W(x_p, \lambda^+, 0)$ is negative in the jumps for any $(x_p, \lambda, \tau) \in \mathcal{A}$. Hence, if the solution to $\mathcal{H}_p$ reaches $\mathcal{A}$, it will remain therein.

Finally, applying the nonsmooth invariance principle given in [38], and using the well posedness result established at the beginning of the proof, leads to the conclusion that, for small enough values of T_p, $\mathcal{A}$ is UGAS.

Proof of (ii): We prove here that the particular solutions included in set $\mathcal{E}_\kappa$ are in $\mathcal{A}$. Remember that the set $\mathcal{E}_\kappa$ consists of the hybrid arcs that start at the origin $x_p = 0$. Then, for every point in $\mathcal{E}_\kappa$

$$\begin{aligned} W(\xi_p) &= \left(e^{\Gamma_\lambda \tau} \begin{bmatrix} 0 \\ 1 \end{bmatrix}\right)^\top \mathcal{P}(\lambda, \tau) \left(e^{\Gamma_\lambda \tau} \begin{bmatrix} 0 \\ 1 \end{bmatrix}\right) \\ &= \left(e^{\Gamma_\lambda \tau} \begin{bmatrix} 0 \\ 1 \end{bmatrix}\right)^\top e^{-\Gamma_\lambda^\top \tau} \mathcal{P}(\lambda, 0) e^{-\Gamma_\lambda \tau} \left(e^{\Gamma_\lambda \tau} \begin{bmatrix} 0 \\ 1 \end{bmatrix}\right) \\ &= \begin{bmatrix} 0 \\ 1 \end{bmatrix}^\top \mathcal{P}(\lambda, 0) \begin{bmatrix} 0 \\ 1 \end{bmatrix} = 0 \leq 1, \end{aligned}$$

which holds for any $(\lambda, \tau) \in [0, 1] \times [0, T_p]$. □

Remark 2: The UGAS property guaranteed for system $\mathcal{H}_p$ implies stability properties for system $\mathcal{H}$, according to Proposition 1.

Remark 3: It is worth noting that the particular case $M = 0$ corresponds to an open-loop control

$$\kappa(x_p) = \lambda_e.$$

Indeed, Theorem (1) proves the UGAS property of the attractor even with this particular control law. Nevertheless, the open-loop character of this case makes this control law unsuitable for practical applications.

V. CONTROLLER PARAMETER TUNING OF THE SYSTEM PERFORMANCE

Now, the question is how to provide performance-based criteria for the selection of M and Q. These matrices can be chosen to improve performance, in terms of current peaks, or even, the chattering amplitude in steady state. To this goal, first a chattering estimation is obtained, and then a discussion about the selection of these matrices is provided.

A. CHATTERING ESTIMATION

It is interesting to have a measure of the amplitude of the chattering in steady state, i.e., once trajectories have entered in $\mathcal{A}$. Theorem 1 guarantees the convergence to $\|x_p\| \leq \varepsilon(T_p)$ when T_p is small enough, but it is desirable to quantify the size of the attractor (related to the amplitude of the chattering) as a function of T_p.

Property 1: Consider Assumption 1 as well as Theorem 1 assumptions are satisfied and a given T_p small enough. Then,

$$\hat{\varepsilon}(T_p) := \frac{2\|B_{\lambda_e}\| \frac{p_M}{\sqrt{p_m}} T_p}{\|\operatorname{He}(PA_{\lambda_e})\| p_M T_p - p_m}, \tag{39}$$

is an approximation of the following upper bound

$$\|x_p^{ss}\| \leq \hat{\varepsilon}(T_p) \quad \forall x_p^{ss} \in \mathcal{A}.$$

where x_p^{ss} denotes the steady state of x_p of system (9)–(10),(16)–(17).

Proof: First, it is easy to see that $W(x_p, \lambda, \tau)$ is decreasing with respect to $\tau \in [0, T_p]$. Moreover, consider T_p small enough and λ_e satisfying Assumption 1 such that the following first-order approximation

$$\begin{aligned} W(x_p, \lambda_e, T_p) &= \begin{bmatrix} x_p^{ss} \\ 1 \end{bmatrix}^\top \left(e^{-\Gamma_{\lambda_e} T_p}\right)^\top \bar{P} e^{-\Gamma_{\lambda_e} T_p} \begin{bmatrix} x_p^{ss} \\ 1 \end{bmatrix} \\ &\approx \begin{bmatrix} x_p^{ss} \\ 1 \end{bmatrix}^\top \begin{bmatrix} P - \operatorname{He}(PA_{\lambda_e}) T_p & -PB_{\lambda_e} T_p \\ -B_{\lambda_e}^\top P T_p & 1 \end{bmatrix} \begin{bmatrix} x_p^{ss} \\ 1 \end{bmatrix} \end{aligned}$$

is obtained applying (31) and neglecting T_p^2. Now, if Theorem 1 assumptions are satisfied, it holds that

$$\begin{aligned} &\begin{bmatrix} x_p^{ss} \\ 1 \end{bmatrix}^\top \begin{bmatrix} P - \operatorname{He}(PA_{\lambda_e}) T_p & -PB_{\lambda_e} T_p \\ -B_{\lambda_e}^\top P T_p & 1 \end{bmatrix} \begin{bmatrix} x_p^{ss} \\ 1 \end{bmatrix} < 1 \\ &\Leftrightarrow 0 < x_p^{ss\top} (\operatorname{He}(PA_{\lambda_e}) T_p - P) x_p^{ss} + 2 x^{ss}{}_p^\top P B_{\lambda_e} T_p \\ &< x_p^{ss\top} (P - \operatorname{He}(PA_{\lambda_e}) T_p) x_p^{ss} + 2 x_p^{ss\top} P B_{\lambda_e} T_p \\ &< (\|1 - \operatorname{He}(A_{\lambda_e})\| \frac{p_M}{p_m} T_p) \|x_p^{ss}\|_P^2 + 2\|B_{\lambda_e}\| \frac{p_M}{\sqrt{p_m}} T_p \|x_p^{ss}\|_P \\ &\Leftrightarrow \|x_p^{ss}\|_P < \frac{2\|B_{\lambda_e}\| \frac{p_M}{\sqrt{p_m}} T_p}{\|\operatorname{He}(A_{\lambda_e})\| \frac{p_M}{p_m} T_p - 1} \\ &\Leftrightarrow \|x_p^{ss}\| < \frac{2\|B_{\lambda_e}\| \frac{p_M}{\sqrt{p_m}} T_p}{\|\operatorname{He}(A_{\lambda_e})\| p_M T_p - p_m} \end{aligned}$$

where p_M and p_m are the maximum and minimum eigenvalues of P and $\|x_p^{ss}\|_P = x^{ss}{}_p^\top P x_p^{ss}$. □

It is worth noting, from Property 1, that if T_p decreases, $\|x_p^{ss}\|$ also decreases.

Property 2: Consider that Assumption 1 is satisfied, and a given T_p small enough such that Property 1 is valid. Then, for

a given positive parameter $\varepsilon > 0$, the state x in steady state, denoted as x^{ss} is limited by

$$\|x^{ss}\| \leq \varepsilon e^{\frac{\alpha T_p}{2}} \tag{40}$$

where $\alpha := 2(a_M + \frac{B_M}{\varepsilon})$ such that $a_M := \frac{1}{2}\max(a_{0,M}, a_{1,M})$ with $a_{i,M}$ the maximum eigenvalue of $|\,\mathrm{He}(A_i)|$ and $B_M := \max(\|B_0\|, \|B_1\|)$. Moreover, $\hat{\varepsilon}$ defined in (39) is an estimation of ε.

Proof: Consider the following variable, $\chi := \|x^{ss}\|^2$, i.e. the squared norm of x in steady state, and note that the dynamics of this variable is bounded from the definition of a_M and B_M,

$$\dot{\chi} = 2x^{ss\top}(A_\sigma x^{ss} + B_\sigma) \leq 2a_M\chi + 2\sqrt{\chi}B_M. \tag{41}$$

Then, in order to find upper bounds on χ in steady state, the worst cases bill be analyzed, i.e., the time subintervals inside the sampling period where $\|x^{ss}\| > \hat{\varepsilon}$ (assuming that Property 1 provides a valid $\hat{\varepsilon}$). Along those intervals,

$$\dot{\chi} \leq 2\alpha\chi \text{ with } \alpha := a_M + \frac{B_M}{\hat{\varepsilon}}. \tag{42}$$

Now, it must be proved that the upper bound on the right hand side of the χ dynamics directly implies the upper boundedness of the solution of (41) by the solution of the bounding equation (42). For this, let us define $\chi_1(t) = \chi(x_0^{ss})e^{2\alpha t}$ as the solution to the bounding equation (42) and $\chi_2(x^{ss}{}_2)$ as the solution to the actual system (41). Then, if $\chi_1(x_0^{ss}) = \chi_2(x_0^{ss})$,

$$\frac{d(\chi_1 - \chi_2)}{dt} = 2\alpha\chi_1 - 2x_2^{ss\top}(A_\sigma x_2^{ss} + B_\sigma) \geq 2\alpha(\chi_1 - \chi_2).$$

This means that χ_1 being greater or equal than χ_2 at some time implies that it will remain so in the future. Note that the inequality comes from (41) and the fact that the focus lies on $\frac{\|x^{ss}\|}{\hat{\varepsilon}} > 1$. If this does not hold, then $\hat{\varepsilon}$ is an even stricter bound than the one that Property 2 suggests. In that case, the integration time of this proof would start when $\|x^{ss}\|$ exits that bounding interval, leaving less time for escaping from it. Finally, $\chi_1(t) \geq \chi_2(t)$ implies that

$$\chi_2(t) \leq \chi(x_0^{ss})e^{2\alpha T_p} \Rightarrow \|x^{ss}\| \leq \hat{\varepsilon}e^{\frac{\alpha T_p}{2}}.$$

In that expression, the bounding exponential $e^{2\alpha t}$ has only been allowed to evolve for a time period of $T_p/2$, as it is the maximum time distance from the interval edges $0, T_p$, where the $\hat{\varepsilon}$ bound holds. It was also assumed $\chi(x_0^{ss}) = \chi_1(x_0^{ss}) = \chi_2(x_0^{ss}) \leq \hat{\varepsilon}^2$, concluding the proof. □

B. DISCUSSION

Theorem 1 establishes stability and performance properties for (4)–(7). Moreover, there are still degrees of freedom in the selection of matrices M and Q, available for closed–loop performance tuning.

1) SELECTION OF Q

On the one hand, for a selected matrix $Q \succ 0 \in \mathbb{R}^n$, the feasibility problem composed of (25)–(26) provides a matrix P necessary to compute the upper bound of $\|x_p^{ss}\|$ defined in Property 1. Hence, the selection of Q can be used to manage the chattering in steady state.

2) SELECTION OF M

On the other hand, this tuning parameter adjusts the transient time, modifying the response time, voltage oscillations, current peak, among others. Indeed, if $M \succ 0$, the system response can be faster and/or can present voltage oscillations, with tendency to saturate the control signal. Conversely, if $M \prec 0$, the system time response can increase, diminishing the current peaks.

VI. SIMULATIONS

Some simulations have been performed to validate the results proposed here. For this, a boost converter has been selected, with the topology shown in Fig. 3. Taking the model given in (1) $z = [i_L\ v_C]^\top$, $\sigma = 0$ when the switch S is closed and $\sigma = 1$ when this switch is open,

$$A_0 = \begin{bmatrix} -R/L & 0 \\ 0 & -1/R_0C_0 \end{bmatrix}, \quad A_1 = \begin{bmatrix} -R/L & -1/L \\ 1/C_0 & -1/R_0C_0 \end{bmatrix},$$
$$\mathcal{B}_0 = \mathcal{B}_1 = \begin{bmatrix} V_{in}/L \\ 0 \end{bmatrix}.$$

The parameters inside these expressions are given in Table 1.

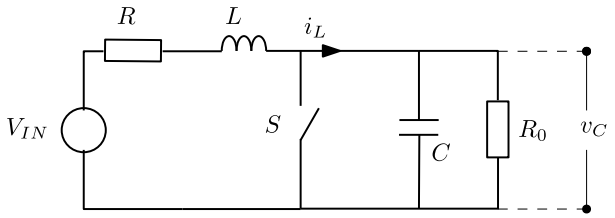

FIGURE 3. Boost converter.

TABLE 1. Boost converter parameters.

COMPONENT	NOMINAL VALUE
V_{in}	24 V
R	5 $m\Omega$
L	470 μH
C	20 μF
R_0	50 Ω

The selected operating point is $x_e = [8.4\ 100]^T$, with its associated $\lambda_e = 0.76$. The simulations are performed with $T_p = 10\mu s$.

The following matrices $Q = \begin{bmatrix} 8.35 & 0.01 \\ 0.01 & 8.33 \end{bmatrix} \cdot 10^3$ and $P = \begin{bmatrix} 416.40 & -0.68 \\ -0.68 & 17.47 \end{bmatrix}$ satisfy the feasibility problem (25)–(26). Now, it is required to adjust matrix M. For this, some simulations have been performed with different choices of M. Fig. 4 compares the state evolutions with

$M = 0.5Q \succ 0$, $M = 0$ and $M = -0.5Q \prec 0$. As mentioned in item 2, Section V-B, if $M \succ 0$ the rise time is reduced, but the control signal will have a tendency to saturate, yielding a strong oscillating behaviour in transient time. In face of this, choosing $M \prec 0$ reduces the current peak and the control input is not saturated, but the system dynamics become slower. Moreover, note that the particular case $M = 0$, provides $\lambda^+ = \lambda_e$, as mentioned in Remark 3. Fig. 5 shows some evolutions with $M \prec 0$. As M is more negative, the response time of the signal is slightly slower. Moreover, with $M \succ 0$, as M is larger the signal control also tends to saturate, as shown in Fig. 6. Note that the control input does not saturate, but the high overshoot generated in the current signal can harm the converter.

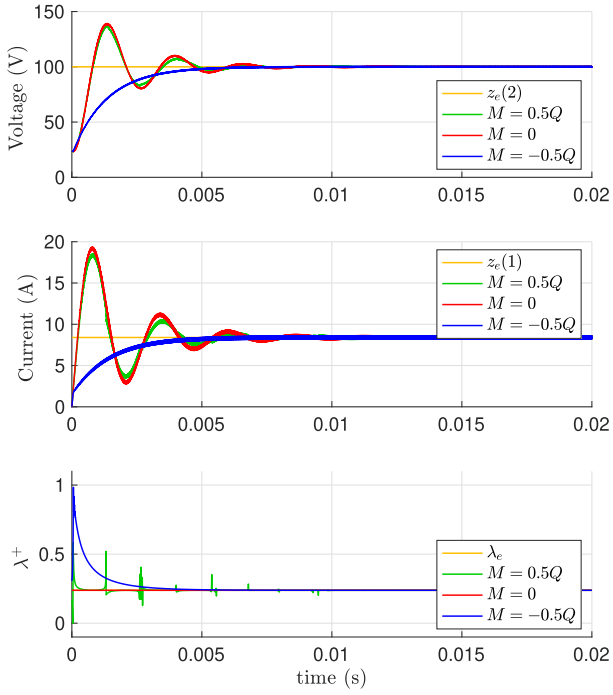

FIGURE 4. State and control input evolutions, choosing $M = 0.5Q$, in green, $M = 0$, in red, and $M = -0.5Q$, in blue.

VII. EXPERIMENTAL SETUP

A test setup was built to validate the proposed hybrid control scheme. Fig. 7 shows this experimental set up. It is composed of:

- A boost converter whose electrical parameters are given in Table 2.
- An electronic card with a current sensor (model LEM LTS 15-NP) for the measurements of the inductor current, and a voltage sensor for the measurement of the output voltage. We built the voltage sensor by means of a resistor divider connected with an operational amplifier in buffer configuration.
- A dSPACE card (DS1103) that includes a PowerPC 604e at 400 MHz and a fixed-point DSP TMS320F240.

The code of the control algorithm was generated by Matlab coder® and it is automatically optimized for running in the dSPACE card.

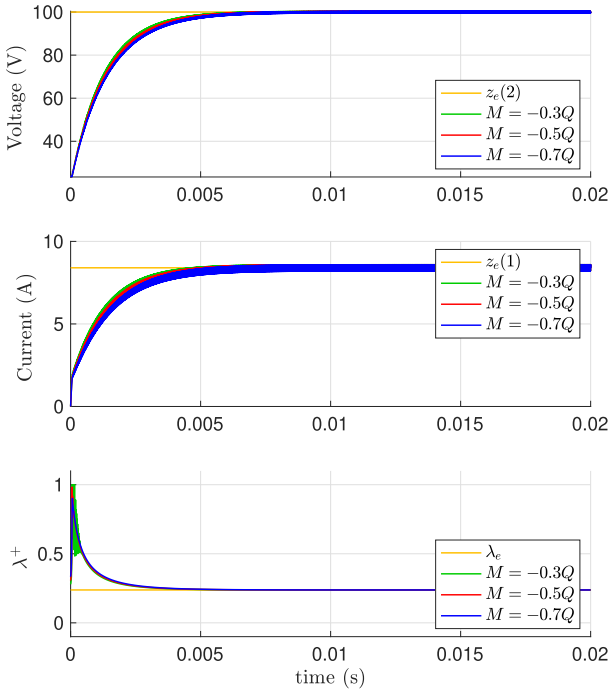

FIGURE 5. State and control input evolutions, choosing $M = -0.3Q$, in green, $M = -0.5Q$, in red, and $M = -0.7Q$, in blue.

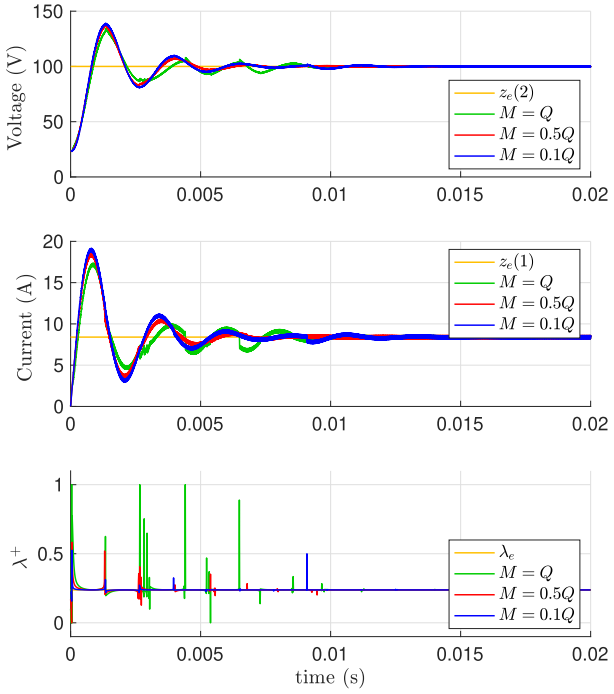

FIGURE 6. State and control input evolutions, choosing $M = Q$, in green, $M = 0.5Q$, in red, and $M = 0.1Q$, in blue.

We selected for these tests $M = -0.5Q$, after several simulation trials. Moreover, the switching frequency was the same than the one taken in the simulation section, 100kHz.

Fig. 8 shows a startup transient from a initial condition equal to $x_0 = \begin{bmatrix} 0 & V_{in} \end{bmatrix}$ to a reference operating point

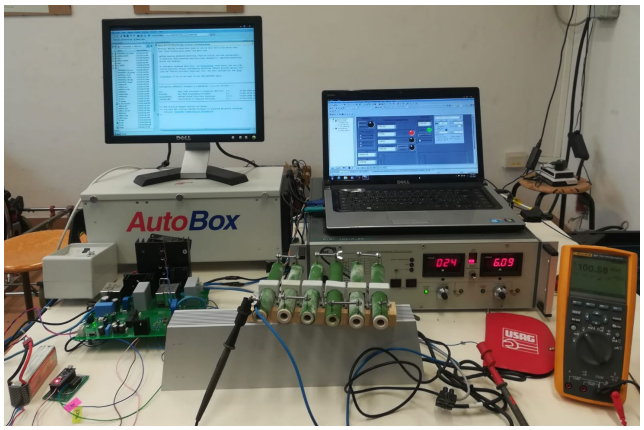

FIGURE 7. Experimental set up.

TABLE 2. Circuit parameters values.

Component	Value	Model
V_{IN}	24V	
L	470μH	AGP4233-474ME
R	11.5mΩ	
C_1	20μF	MKP1848C62090JP4
R_C	5mΩ	
R_0	50Ω	
Diode		C3D06060A
Switch		C3M0065090D
Driver		1EDI20N12AF

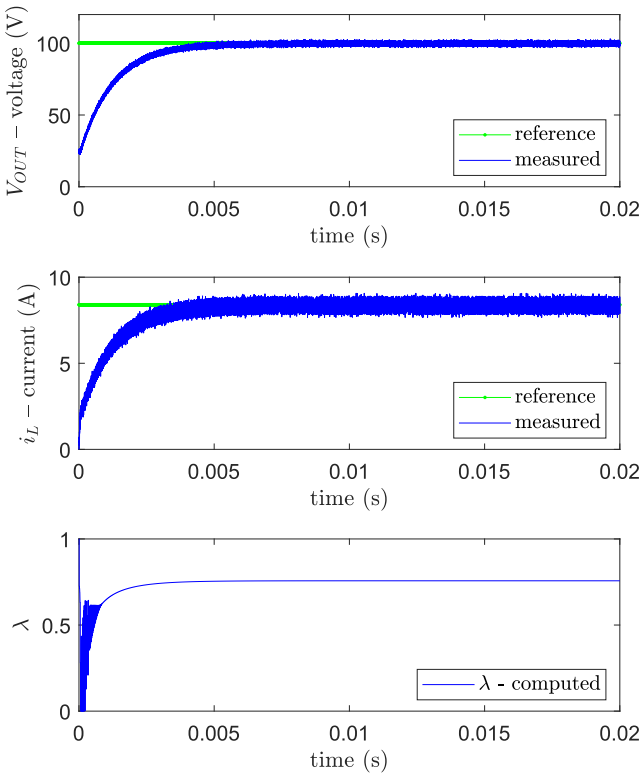

FIGURE 8. Evolutions of the voltage, current and duty cycle in the start up.

computed by imposing an output voltage equal to $V_{out} = 100$V. The voltage and current signals present a smooth behaviour without current peaks, as shown in simulation

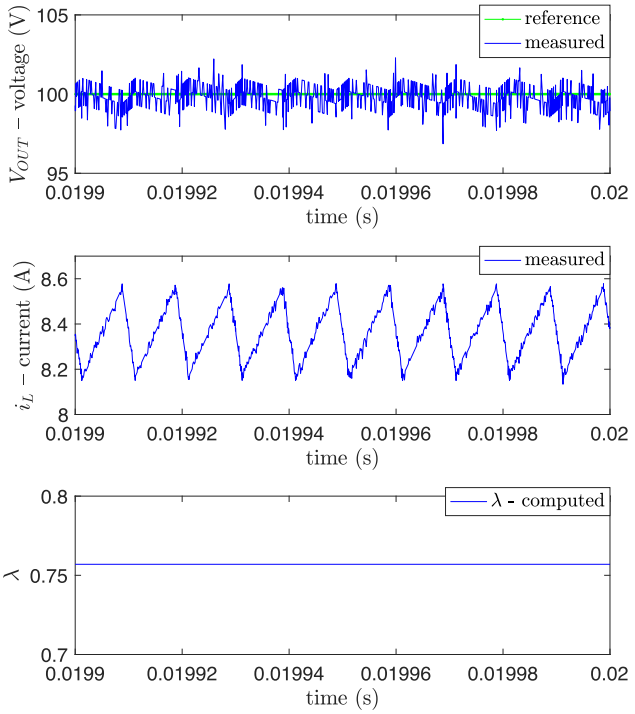

FIGURE 9. Evolutions of the voltage, current and duty cycle in the steady state.

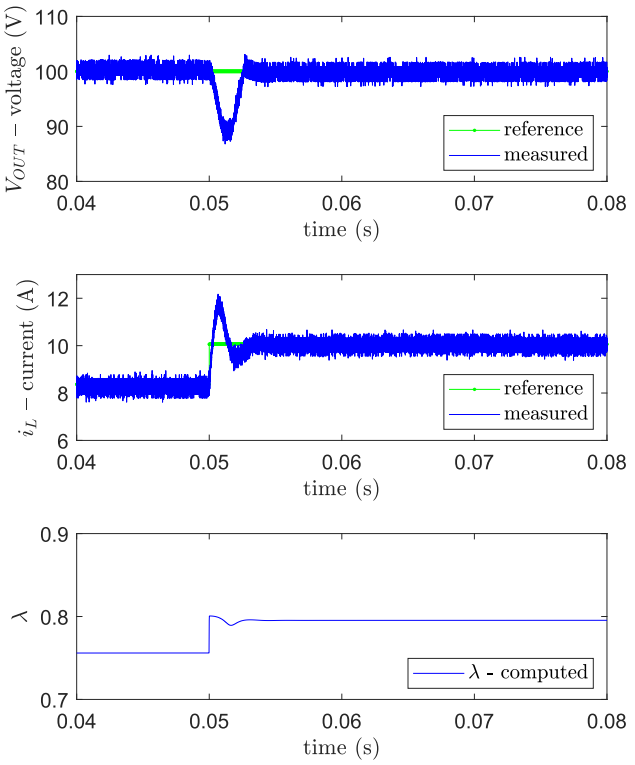

FIGURE 10. Evolutions of the voltage, current and duty cycle for regulating the voltage output with a perturbation of V_{in}.

(see Fig. 4). Likewise, the steady-state operation is shown in Fig. 9. The measured errors of the voltage and current provide $\|x^{ss}\| = 3.01$, whereas the computed estimated upper bound of (40) is $\hat{\varepsilon} = 3.54$ and $\varepsilon e^{\frac{\alpha T_p}{2}} = 9.77$.

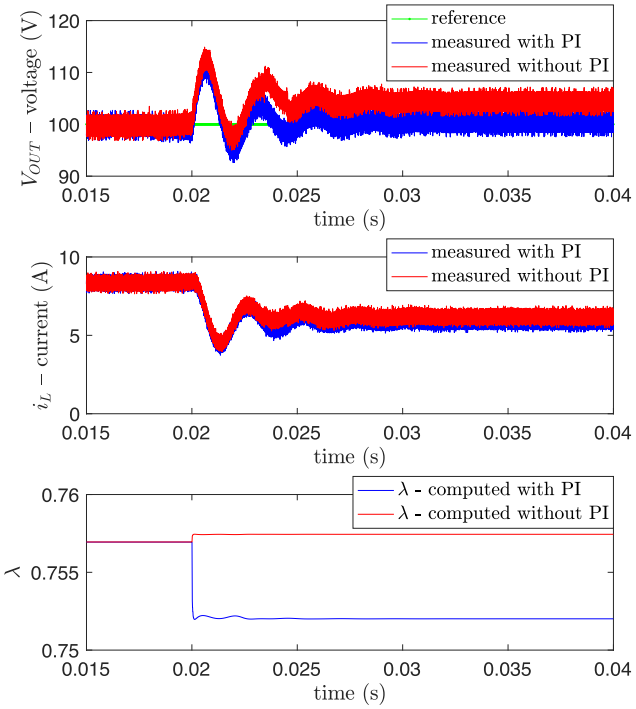

FIGURE 11. Evolutions of the voltage, current and duty cycle without PI controller (in red) and with PI controller (in blue) for regulating the voltage output with a perturbation of R_0.

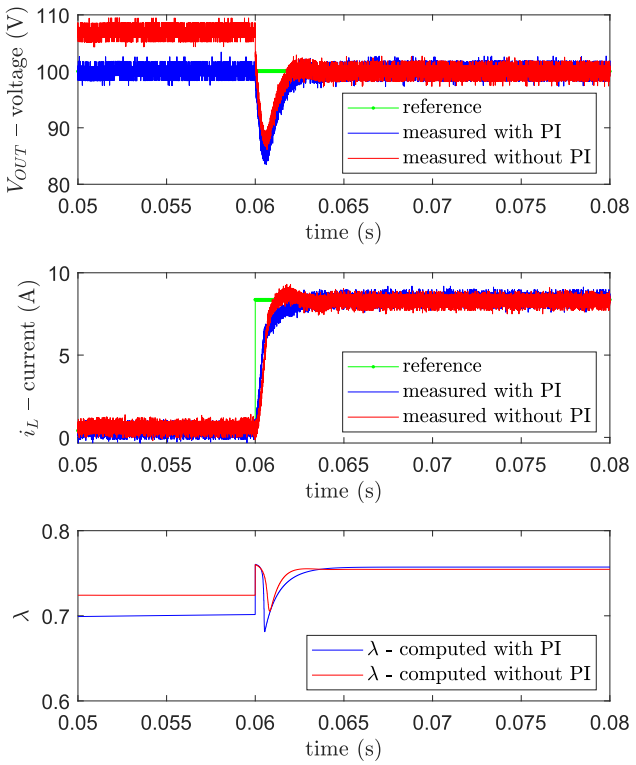

FIGURE 12. Evolutions of the voltage, current and duty cycle without PI controller (in red) and with PI controller (in blue) during a transition from no load to rated load.

In order to verify robustness of the proposed control system and to test its dynamic response in some different scenarios, three tests have been performed. In the first one, the input voltage is changed from 24V to 20V and the results are given in Fig. 10. This figure shows the ability of the system of ensuring an output voltage regulation even when an input voltage variation occurs. In a second test, the load R_0 was changed from $R_0 = 50\Omega$ to $R_0 = 75\Omega$ at $t = 0.02$s (see Fig. 11). Note that here, differently from the previous test where the input voltage variation was easily measured and used in the computation of the new equilibrium point, the resistance value cannot be measured, and an error in the voltage output can be exhibited in steady state. This is due to the fact that the proposed algorithm does not guarantee an output voltage regulation when a load variation happens. However, if an external loop is added with a PI controller as in [39], the output voltage is regulated at its reference value, maintaining a suited performance as shown in Fig. 11. Finally, Fig. 12 shows the variable trajectories when the system suffers a perturbation due to a transition from no-load to the nominal one. The new test is more challenging because there is a 100% variation of the nominal load.

VIII. CONCLUSION

A hybrid model of switched power converters composed of two functioning modes, triangular-carrier PWM inputs and a sample-and-hold mechanism has been presented here. This study can be extended to other power converters with more than two functioning modes. The dynamic equations are then simplified to an equivalent system with trajectories that match those of the original one at the start of the sampling intervals, but with fewer jumps than the original one, and a reduced state vector. Moreover, a rigorous control law to select the value of the duty cycle at the beginning of each PWM-sampling interval has been proposed. Stability in closed loop has been established via hybrid dynamical systems theory. Finally, an estimation of the chattering peaks reached by the system state is provided. Experimental results show satisfactory closed-loop performance.

PWMs with more than 2 modes will be considered in future works. Moreover, a stability analysis with an external control loop that controls the output voltage is also expected.

REFERENCES

[1] R. D. Middlebrook, "Small-signal modeling of pulse-width modulated switched-mode power converters," *Proc. IEEE*, vol. 76, no. 4, pp. 343–354, Apr. 1988.
[2] O. Ali Beg, H. Abbas, T. T. Johnson, and A. Davoudi, "Model validation of PWM DC–DC converters," *IEEE Trans. Ind. Electron.*, vol. 64, no. 9, pp. 7049–7059, Sep. 2017.
[3] A. Antonopoulos, L. Angquist, and H. P. Nee, "On dynamics and voltage control of the modular multilevel converter," in *Proc. IEEE Eur. Conf. Power Electron. Appl.*, Sep. 2009, pp. 3353–3362.
[4] R. D. Middlebrook and S. Cuk, "A general unified approach to modelling switching-converter power stages," in *Proc. IEEE Power Electron. Spec. Conf.*, Jun. 1976, pp. 18–34.
[5] H. J. Sira-Ramirez and R. Silva-Ortigoza, *Control Design Techniques in Power Electronics Devices*. London, U.K.: Springer, 2006.
[6] D. G. Holmes and T. A. Lipo, *Pulse Width Modulation for Power Converters: Principles and Practice*, vol. 18. Hoboken, NJ, USA: Wiley, 2003.
[7] S. K. Peddapelli, *Pulse Width Modulation. Other Titles in Applied Mathematics*. Berlin, Germany: De Gruyter Oldenbourg, 2016.

[8] S. Mariéthoz, S. Almér, M. Bâja, A. G. Beccuti, D. Patino, A. Wernrud, J. Buisson, H. Cormerais, T. Geyer, H. Fujioka, and U. T. Jonsson, "Comparison of hybrid control techniques for buck and boost DC–DC converters," *IEEE Trans. Control Syst. Technol.*, vol. 18, no. 5, pp. 1126–1145, Sep. 2010.

[9] E. Vidal-Idiarte, A. Marcos-Pastor, G. Garcia, A. Cid-Pastor, and L. Martinez-Salamero, "Discrete-time sliding-mode-based digital pulse width modulation control of a boost converter," *IET Power Electron.*, vol. 8, no. 5, pp. 708–714, May 2015.

[10] P. Cortés, M. P. Kazmierkowski, R. M. Kennel, D. E. Quevedo, and J. Rodríguez, "Predictive control in power electronics and drives," *IEEE Trans. Ind. Electron.*, vol. 55, no. 12, pp. 4312–4324, Dec. 2008.

[11] G. S. Deaecto, J. C. Geromel, F. S. Garcia, and J. A. Pomilio, "Switched affine systems control design with application to DC–DC converters," *IET Control Theory Appl.*, vol. 4, no. 7, pp. 1201–1210, 2010.

[12] L. Hetel and E. Fridman, "Robust sampled—Data control of switched affine systems," *IEEE Trans. Autom. Control*, vol. 58, no. 11, pp. 2922–2928, Nov. 2013.

[13] L. Martinez-Salamero, G. García, C. Orellana, M. Lahore, B. Estibals, C. Alonso, and E. C. Carrejo, "Analysis and design of a sliding-mode strategy for start-up control and voltage regulation in a buck converter," *IET Power Electron.*, vol. 6, no. 1, pp. 52–59, Jan. 2013.

[14] R. Goebel, R. G. Sanfelice, and A. R. Teel, *Hybrid Dynamical Systems: Modeling, Stability, and Robustness*. Princeton, NJ, USA: Princeton Univ. Press, 2012.

[15] R. A. DeCarlo, M. S. Branicky, S. Pettersson, and B. Lennartson, "Perspectives and results on the stability and stabilizability of hybrid systems," *Proc. IEEE*, vol. 88, no. 7, pp. 1069–1082, Jul. 2000.

[16] D. Liberzon and A. S. Morse, "Basic problems in stability and design of switched systems," *IEEE Control Syst.*, vol. 19, no. 5, pp. 59–70, Oct. 1999.

[17] D. Liberzon, *Switching in Systems and Control. Other Titles in Applied Mathematics*. Boston, MA, USA: Springer, 2003.

[18] R. Goebel, R. G. Sanfelice, and A. Teel, "Hybrid dynamical systems," *IEEE Control Syst. Mag.*, vol. 29, no. 2, pp. 28–93, Apr. 2009.

[19] T. A. F. Theunisse, J. Chai, R. G. Sanfelice, and W. P. M. H. Heemels, "Robust global stabilization of the DC–DC boost converter via hybrid control," *IEEE Trans. Circuits Syst. I, Reg. Papers*, vol. 62, no. 4, pp. 1052–1061, Apr. 2015.

[20] C. Albea, G. Garcia, and L. Zaccarian, "Hybrid dynamic modeling and control of switched affine systems: Application to DC–DC converters," in *Proc. 54th IEEE Conf. Decis. Control (CDC)*, Dec. 2015, pp. 2264–2269. [Online]. Available: https://hal.archives-ouvertes.fr/hal-01220447v3/document.

[21] A. Sferlazza, C. Albea-Sanchez, and G. Garcia, "A hybrid control strategy for quadratic boost converters with inductor currents estimation," *Control Eng. Pract.*, vol. 103, Oct. 2020, Art. no. 104602.

[22] L. Torquati, R. G. Sanfelice, and L. Zaccarian, "A hybrid predictive control algorithm for tracking in a single-phase DC/AC inverter," in *Proc. IEEE Conf. Control Technol. Appl. (CCTA)*, Aug. 2017, pp. 904–909.

[23] C. A. Sanchez, G. Garcia, S. Hadjeras, W. P. M. H. Heemels, and L. Zaccarian, "Practical stabilization of switched affine systems with dwell-time guarantees," *IEEE Trans. Autom. Control*, vol. 64, no. 11, pp. 4811–4817, Nov. 2019.

[24] C. Albea and A. Seuret, "Time-triggered and event-triggered control of switched affine systems via a hybrid dynamical approach," *Nonlinear Anal., Hybrid Syst.*, vol. 41, Aug. 2021, Art. no. 101039.

[25] J. Chai and R. G. Sanfelice, "A robust hybrid control algorithm for a single-phase DC/AC inverter with variable input voltage," in *Proc. Amer. Control Conf.*, Jun. 2014, pp. 1420–1425.

[26] A. R. Teel and D. Nesic, "PWM hybrid control systems: Averaging tools for analysis and design," in *Proc. IEEE Int. Conf. Control Appl.*, Sep. 2010, pp. 1128–1133.

[27] C. Albea, A. Sferlazza, F. Gordillo, and F. Gomez-Estern, "Control of power converters with hybrid affine models and pulse-width modulated inputs," *IEEE Trans. Circuits Syst. I, Reg. Papers*, vol. 68, no. 8, pp. 3485–3494, Aug. 2021, doi: 10.1109/TCSI.2021.3083900.

[28] M. Tariq, M. Meraj, A. Azeem, A. I. Maswood, A. Iqbal, and B. Chokkalingam, "Evaluation of level-shifted and phase-shifted PWM schemes for seven level single-phase packed u cell inverter," *CPSS Trans. Power Electron. Appl.*, vol. 3, no. 3, pp. 232–242, Sep. 2018.

[29] S. da Silva Carvalho, M. Halamicek, N. Vukadinovic, and A. Prodic, "Digital PWM for multi-level flying capacitor converters with improved output resolution and flying capacitor voltage controller stability," in *Proc. IEEE 19th Workshop Control Modeling Power Electron. (COMPEL)*, Jun. 2018, pp. 1–7.

[30] P. S. Gurpide, O. A. Sadaba, L. M. Palomo, T. Meynard, and E. Lefeuvre, "A new control strategy for the boost DC-AC inverter," in *Proc. IEEE 32nd Annu. Power Electron. Spec. Conf.*, Jun. 2001, pp. 974–979.

[31] A. Bouafia, F. Krim, and J.-P. Gaubert, "Design and implementation of high performance direct power control of three-phase PWM rectifier, via fuzzy and PI controller for output voltage regulation," *Energy Convers. Manage.*, vol. 50, no. 1, pp. 6–13, Jan. 2009.

[32] H. Kanaan, K. Al-Haddad, and F. Fnaiech, "Modelling and control of three-phase/switch/level fixed-frequency PWM rectifier: State-space averaged model," *IEE Proc.-Electr. Power Appl.*, vol. 152, no. 3, pp. 551–557, May 2005.

[33] A. Yazdani and R. Iravani, "A generalized state-space averaged model of the three-level NPC converter for systematic DC-voltage-balancer and current-controller design," *IEEE Trans. Power Del.*, vol. 20, no. 2, pp. 1105–1114, Apr. 2005.

[34] P. Handley and J. Boys, "Practical real-time PWM modulators: An assessment," *IEE Proc. B, Electr. Power Appl.*, vol. 139, pp. 96–102, Mar. 1992.

[35] A. F. Filippov, *Differential Equations With Discontinuous Righthand Sides: Control Systems*, vol. 18. Boston, MA, USA: Springer, 2013.

[36] D. J. Perreault and G. C. Verghese, "Time-varying effects and averaging issues in models for current-mode control," *IEEE Trans. Power Electron.*, vol. 12, no. 3, pp. 453–461, May 1997.

[37] L. Iannelli, K. Henrik Johansson, U. T. Jönsson, and F. Vasca, "Subtleties in the averaging of a class of hybrid systems with applications to power converters," *Control Eng. Pract.*, vol. 16, no. 8, pp. 961–975, Aug. 2008.

[38] A. Seuret, C. Prieur, S. Tarbouriech, A. R. Teel, and L. Zaccarian, "A non-smooth hybrid invariance principle applied to robust event-triggered design," *IEEE Trans. Autom. Control*, vol. 64, no. 5, pp. 2061–2068, May 2019.

[39] A. Sferlazza, C. Albea-Sanchez, L. Martinez-Salamero, G. Garcia, and C. Alonso, "Min-type control strategy of a DC–DC synchronous boost converter," *IEEE Trans. Ind. Electron.*, vol. 67, no. 4, pp. 3167–3179, Apr. 2020.

CAROLINA ALBEA received the Ph.D. degree in automatic control from the University of Sevilla, Spain, and the University of Grenoble, France, respectively, in 2010. From 2010 to 2011, she held a postdoctoral position with the CEA-LETI Minatec Campus, Grenoble, France, on the control of nanoelectronic circuits. From 2011 to 2020, she became an Associate Professor with the University of Toulouse III (Université Paul Sabatier) and her research was performed with the LAAS-CNRS. Since 2020, she has been joined the University of Seville, Spain, where she is currently an Associate Professor. Her research interests include hybrid control of switched systems, hybrid dynamical systems application, distributed control, and control of electronic converters.

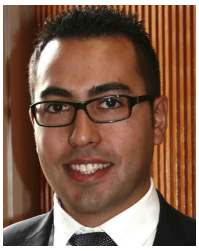

ANTONINO SFERLAZZA (Member, IEEE) was born in Palermo, Italy, in 1987. He received the master's degree in automation engineering and the Ph.D. degree in mathematics and automation from the University of Palermo, Italy, in 2011 and 2015, respectively. In 2013, he was a Visiting Ph.D. student with the University of California at Santa Barbara, Santa Barbara, CA, USA. From 2016 to 2017, he joined the University of Palermo as a Junior Researcher. From 2017 to 2018, he was a Researcher with the LAAS CNRS, Toulouse, France. He is currently a Researcher in systems and control engineering with the University of Palermo. His research interests include the development of feedback control algorithms for nonlinear dynamical systems, estimation theory, and applications of control of electrical drives, power converters, and mechanical systems.

FABIO GÓMEZ-ESTERN received the B.Sc. degree in economics from the University of London, the B.Sc. and M.Sc. degrees in telecommunications engineering from the University of Seville, and the M.Sc. and Ph.D. degrees in control systems from the University of Seville. He has worked in industry, such as Abengoa and France Telecom and as a Visiting Researcher in several European laboratories. From 2002 to 2012, he has been an Associate Professor with the University of Seville, where he has worked as the Head of the Department of Automatic Control. He is currently a Full Professor and the Founding Director of the School of Engineering, Universidad Loyola Andalucía, Seville, Spain. His research interests include nonlinear control systems, distributed control and networked control, with applications to electromechanical systems, and power converters.

FRANCISCO GORDILLO received the M.Eng. and Ph.D. degrees in industrial engineering from the University of Seville, Seville, Spain, in 1988 and 1994, respectively. Since 1989, he has been with the Department of Automatic Control, Escuela Superior de Ingenieros, Universidad de Sevilla, where he is currently a Full Professor. He is the coauthor of Dinamica de Sistemas (Madrid: Alianza Editorial, 1997), a Co-Editor of Stability Issues in Fuzzy Control (Berlin: Physica-Verlag, 2000), and author or coauthor of more than 150 publications, including book chapters, journal articles, and conference proceedings. His research interests include nonlinear control with applications to mechanical, electromechanical, and power electronic systems.